# Supporting Information

## Shedding X-ray Light on the Interfacial Electrochemistry of Silicon Anodes for Li-Ion Batteries

*Chuntian Cao[1,2], Badri Shyam[1], Jiajun Wang[2], Michael F. Toney[1,]*, Hans-Georg Steinrück[1,]**

[1]SSRL Materials Science Division, SLAC National Accelerator Laboratory, Menlo Park, California 94025, United States

[2]School of Chemistry and Chemical Engineering, Harbin Institute of Technology, Harbin, Heilongjiang 150001, China

*E-mail: mftoney@slac.stanford.edu, hgs@slac.stanford.edu

## 1. Parameter confidence analysis:

In order to obtain confidence intervals for the fitting parameters in our X-ray reflectivity (XRR) model refinement, we applied a Monte Carlo resampling technique[1-3]. Here, $N$ independent datasets are randomly synthesized within the experimental data point uncertainties. The same slab-model is then used to fit each of the generated dataset, resulting in $N$ sets of parameters. The error bar of each parameter is subsequently calculated from the standard deviation of the $N$ parameter values. We performed this procedure for each data set.

## 2. Figure of merit:

Typical figures of merit (FOMs) in XRR fitting[4-7] are a "normalized" FOM, $\mathrm{FOM_{normlz}} = \sum_i[(R_i^{\mathrm{model}} - R_i^{\mathrm{data}})/R_i^{\mathrm{data}}]^2$, and a logarithmic FOM, $\mathrm{FOM_{log}} = \sum_i\left(\log R_i^{\mathrm{model}} - \log R_i^{\mathrm{data}}\right)^2$ (or alternatively, $\mathrm{FOM_{log}} = \sum_i |\log R_i^{\mathrm{model}} - \log R_i^{\mathrm{data}}|$). In these equations, $R^{\mathrm{data}}$ and $R^{\mathrm{model}}$ are the measured and calculated/fitted reflectivity, and each "$i$" represents one data point. These FOMs were utilized in our fitting routines, and are usually preferred over chi-square goodness of fit tests as XRR data is spread over a large $x$- and (particularly) $y$-range, where $x = q_z$, and $y$ = reflectivity. If the electron density profile is robust, they yield largely equivalent fitting results, i.e. the fitting results using either of the two FOMs are within the error bar of each other. This is shown in the Figure S1, where we compare the XRR fit and corresponding electron density profile using the $\mathrm{FOM_{normlz}}$ and $\mathrm{FOM_{log}}$, respectively, to refine the 0.2 V dataset from low-potential sequence. The corresponding fit-parameters are shown in Table S1.

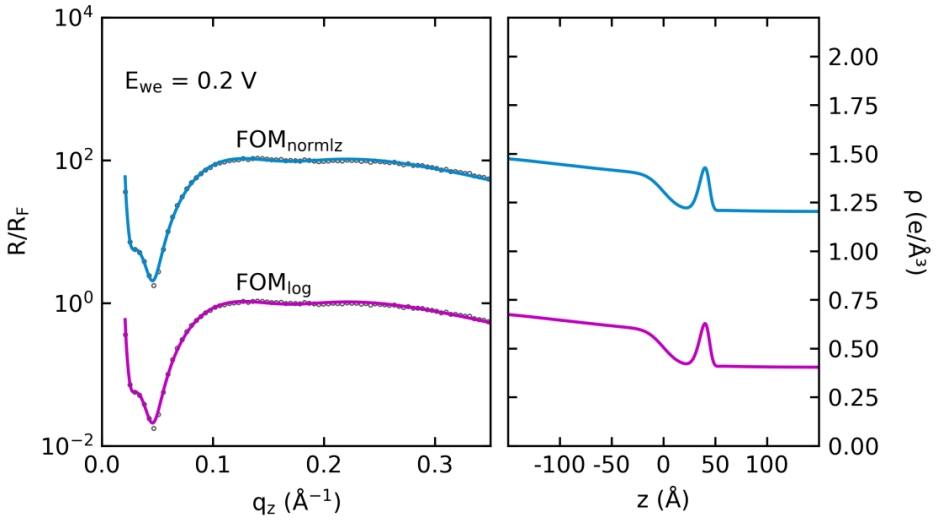


**Figure S1. Comparison of fits using $\mathrm{FOM_{normlz}}$ and $\mathrm{FOM_{log}}$ to fit the 0.2 V dataset from low-potential sequence (see Fig. 2 in main manuscript).**

**Table S1. Best-fit parameter values corresponding to Fig. S2**

| FOM | Top-SEI layer | | | Bottom-SEI layer | | |
|---|---|---|---|---|---|---|
| | Thickness (Å) | Electron density (e/Å$^3$) | Roughness (Å) | Thickness (Å) | Electron density (e/Å$^3$) | Roughness (Å) |
| normlz | 7.1 ±0.5 | 0.78 ±0.02 | 3.1 ±0.1 | 37.1 ±0.4 | 0.40 ±0.01 | 6.4 ±0.3 |
| log | 7.1 ±0.4 | 0.78 ±0.02 | 3.2 ±0.1 | 37.0 ±0.3 | 0.40 ±0.01 | 6.4 ±0.3 |

## 3. Fitting program and fitting algorithm:

GenX[5] and python-based in-house software were used in the XRR model refinement. These use differential evolution[8] algorithms and basin-hopping[9] algorithms, respectively, to provide optimized parameters. These algorithms have the advantage of being robust in finding global minima, whereas more standard Levenberg–Marquardt algorithms often find only a local minimum.

## 4. Resolution:

The resolution of XRR equals $\pi/q_{z_{max}}$, determined by the maximum measured scattering vector $q_{z_{max}}$.[10] This resolution refers to the minimum resolvable layer thickness, while the accuracy in the determination of layer thicker than $\pi/q_{z_{max}}$ can be more precise and depends on the data quality, such as counting statistics and $q_z$-resolution.[11] In our case, $q_{z_{max}}$ ranges from 0.3 - 0.5 Å$^{-1}$, providing a resolution of approximately 6-10 Å, which justifies the utilization of all slabs in our XRR model refinement in terms of resolution.

## 5. Justification of slab-models:

An acceptable model refinement of XRR data must fulfill the following three conditions. (A) Must fit the data well (FOM and eye inspection), and cannot be described to the same accuracy with fewer layers. The more equivalent data sets, in our case in terms of reaction regime, can be described by the same model fits, the more robust the model refinement. (B) Must have physically meaningful and interpretable parameters. (C) The parameters must be within the experimental resolution.

We use three main models in our manuscript to describe XRR curves corresponding to various reaction regimes in the interfacial electrochemistry of silicon:

1. Top-SEI/bottom-SEI/initial-$Li_xSi$ model, used in SEI growth (section 3.1)
2. SEI/$Li_xSi$/dense-Si, used in c-Si lithiation (section 3.2)
3. SEI/Li-dip/$Li_xSi$, used in Si delithiation and a-Si lithiation (section 3.3)

Each layer has a physical meaning, and a description of their justification in terms of comparison of fits using models of increasing complexity is provided in our previous papers[3,12,13]. For ease of comprehension, we briefly summarize the tests for (A) again here via the comparison of fits using different layers. For a detailed discussion of the superiority of the final model over the other tested models we refer the reader to references[3,12,13].

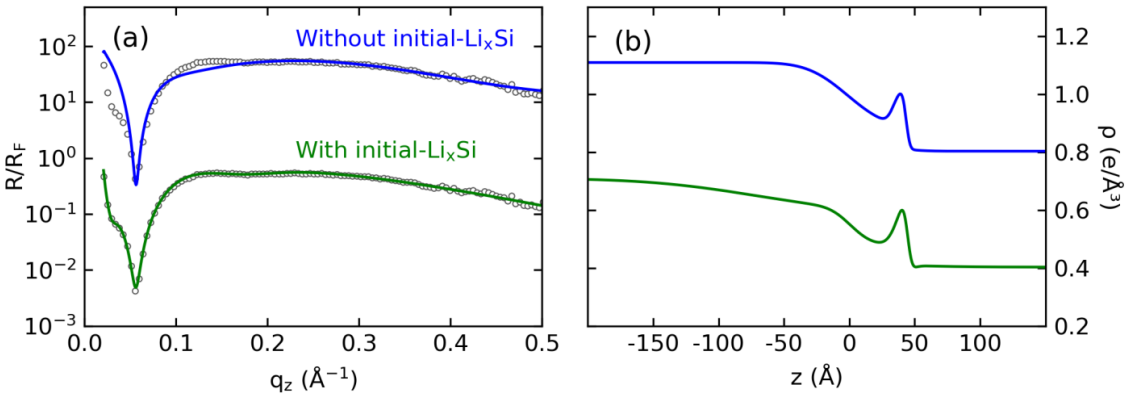


**Figure S2. Justification of the initial-$Li_xSi$ layer during SEI growth (for details see Ref [12]). Adapted with permission from Ref [12]. Copyright 2019 Elsevier.**

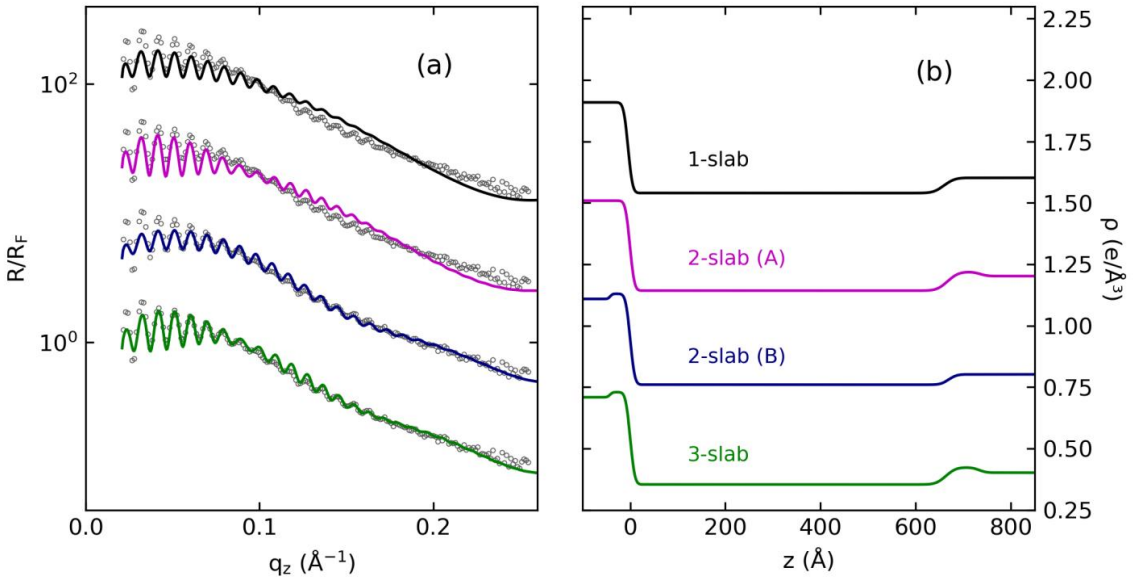


**Figure S3. Justification of the 3-layer model used in c-Si lithiation (for details see Ref [3]). Adapted with permission from Ref [3]. Copyright 2016 American Chemical Society.**

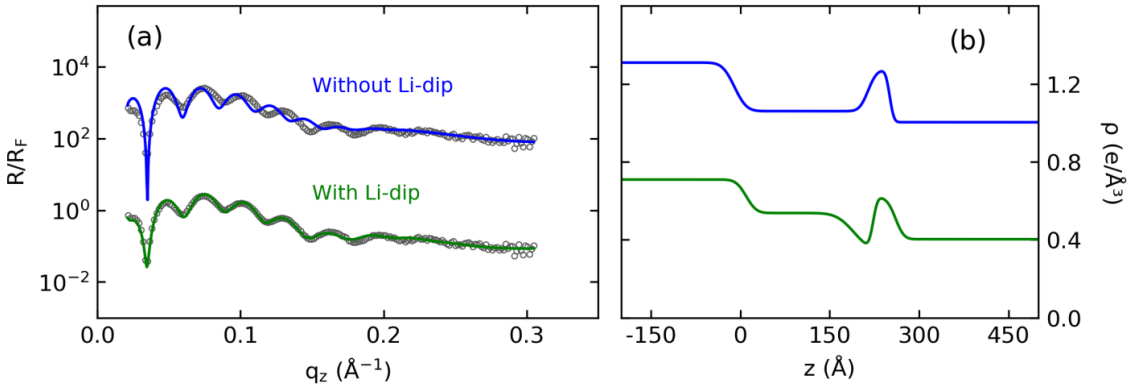


**Figure S4. Justification of the Li-dip layer during Li$_x$Si delithiation and a-Si lithiation (for details see Ref [13]). Adapted with permission from Ref [13]. Copyright 2017 Wiley-VCH.**

## 6. The influence of absorption

As shown in Fig. S5, absorption has an only minor effect on the reflectivity profile, in particular at X-ray energies of 11.5 keV and in the case of mostly light elements such as Si, C, Li, F, and O. Due to the complexity in refining the absorption part in XRR due to the unknown layer composition, we did not vary these parameters, keeping the values fixed at the initial guesses.

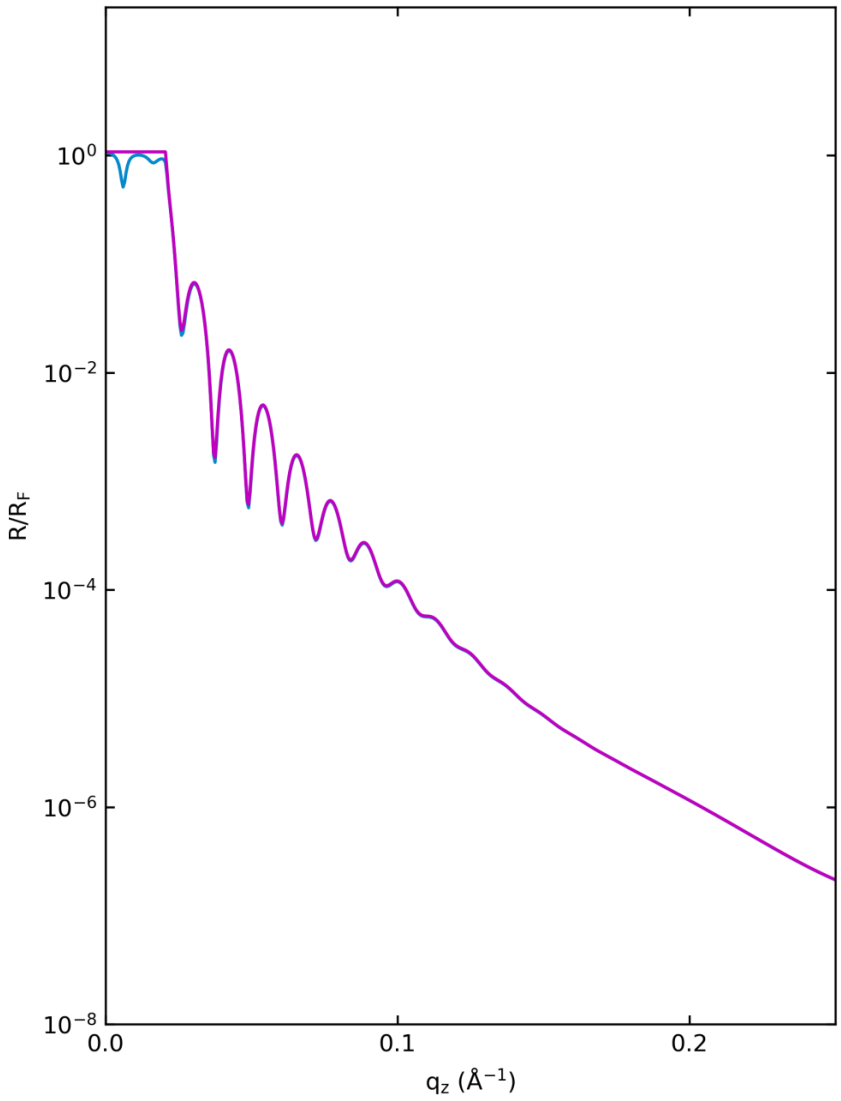


**Figure S5. Comparison of the effect of absorption in the model refinement. Blue: with absorption; Magenta: without absorption.**

**References**


(1) Heinrich, F.; Ng, T.; Vanderah, D. J.; Shekhar, P.; Mihailescu, M.; Nanda, H.; Lösche, M. A new lipid anchor for sparsely tethered bilayer lipid membranes. *Langmuir* 2009, *25*, 4219-4229.

(2) Khassanov, A.; Steinrück, H.-G.; Schmaltz, T.; Magerl, A.; Halik, M. Structural investigations of self-assembled monolayers for organic electronics: results from X-ray reflectivity. *Acc. Chem. Res.* 2015, *48*, 1901-1908.

(3) Cao, C.; Steinrück, H. G.; Shyam, B.; Stone, K. H.; Toney, M. F. In Situ Study of Silicon Electrode Lithiation with X-ray Reflectivity. *Nano Lett.* 2016, *16*, 7394-7401.

(4) Vignaud, G.; Gibaud, A. REFLEX: a program for the analysis of specular X-ray and neutron reflectivity data. *J. Appl. Crystallogr.* 2019, *52*, 201-213.

(5) Björck, M.; Andersson, G. GenX: an extensible X-ray reflectivity refinement program utilizing differential evolution. *J. Appl. Crystallogr.* 2007, *40*, 1174-1178.

(6) Toney, M. F.; Brennan, S. Measurements of carbon thin films using x-ray reflectivity. *J. Appl. Phys.* 1989, *66*, 1861-1863.

(7) Jenkins, R.; Gilfrich, J. V. Figures-of-merit, their philosophy, design and use. *X-Ray Spectrom.* 1992, *21*, 263-269.

(8) Storn, R.; Price, K. J. J. o. G. O. Differential Evolution – A Simple and Efficient Heuristic for global Optimization over Continuous Spaces. 1997, *11*, 341-359.

(9) Wales, D. J.; Doye, J. P. K. Global Optimization by Basin-Hopping and the Lowest Energy Structures of Lennard-Jones Clusters Containing up to 110 Atoms. *The Journal of Physical Chemistry A* 1997, *101*, 5111-5116.

(10) Bracco, J. N.; Lee, S. S.; Stubbs, J. E.; Eng, P. J.; Heberling, F.; Fenter, P.; Stack, A. G. Hydration Structure of the Barite (001)–Water Interface: Comparison of X-ray Reflectivity with Molecular Dynamics Simulations. *J. Phys. Chem. C* 2017, *121*, 12236-12248.

(11) Fenter, P.; Schreiber, F.; Bulović, V.; Forrest, S. Thermally induced failure mechanisms of organic light emitting device structures probed by X-ray specular reflectivity. *Chem. Phys. Lett.* 1997, *277*, 521-526.

(12) Cao, C.; Abate, I. I.; Sivonxay, E.; Shyam, B.; Jia, C.; Moritz, B.; Devereaux, T. P.; Persson, K. A.; Steinrück, H.-G.; Toney, M. F. Solid Electrolyte Interphase on Native Oxide-Terminated Silicon Anodes for Li-Ion Batteries. *Joule* 2019, *3*, 762-781.

(13) Cao, C.; Steinrück, H.-G.; Shyam, B.; Toney, M. F. The Atomic Scale Electrochemical Lithiation and Delithiation Process of Silicon. *Adv. Mater. Interfaces* 2017, 1700771.